Advanced SuperDARN meteor wind observations based on raw time series analysis technique

M. Tsutsumi,[1] A. S. Yukimatu,[1] D. A. Holdsworth,[2] and M. Lester[3]

[1]   The meteor observation technique based on SuperDARN raw time series analysis has been upgraded. This technique extracts meteor information as biproducts and does not degrade the quality of normal SuperDARN operations. In the upgrade the radar operating system (RADOPS) has been modified so that it can oversample every 15 km during the normal operations, which have a range resolution of 45 km. As an alternative method for better range determination a frequency domain interferometry (FDI) capability was also coded in RADOPS, where the operating radio frequency can be changed every pulse sequence. Test observations were conducted using the CUTLASS Iceland East and Finland radars, where oversampling and FDI operation (two frequencies separated by 3 kHz) were simultaneously carried out. Meteor ranges obtained in both ranging techniques agreed very well. The ranges were then combined with the interferometer data to estimate meteor echo reflection heights. Although there were still some ambiguities in the arrival angles of echoes because of the rather long antenna spacing of the interferometers, the heights and arrival angles of most of meteor echoes were more accurately determined than previously. Wind velocities were successfully estimated over the height range of 84 to 110 km. The FDI technique developed here can be further applied to the common SuperDARN operation, and study of fine horizontal structures of F region plasma irregularities is expected in the future.

1. Introduction

[2] The global structure of the mesosphere and lower ionosphere is still poorly understood simply due to the lack of observation sites, although considerable effort has been made to increase the number. Even the longitudinal structure of background winds, including the existence of stationary waves, is not known very well in contrast to the lower atmosphere.

[3] The SuperDARN community has been trying to detect meteors and deduce wind information using their radars widely covering both Arctic and Antarctic regions and conduct network observations in the high latitudes [e.g., *Hall et al.*, 1997]. Most of these radars consist of two one-dimensional arrays; a main array of 16 log-periodic antennas for both transmission and reception and a subarray of 4 antennas for reception only. The antenna pattern is fan shaped with a maximum gain toward the bore site of the log-periodic antennas and the beam can be steered in 16 directions. A multipulse technique is used to produce autocorrelation function (ACF) measurements from a set of unevenly spaced seven pulses which are transmitted every pulse sequence of about 100 ms long. Usually the beam direction is switched every several seconds and all the 16 directions are sampled every few minutes. The SuperDARN radars, however, are originally designed for polar F region ionospheric studies [*Greenwald et al.*, 1985, 1995; *Chisham et al.*, 2007] and the ACF technique is not necessarily suitable for meteor echo observations.

[4] To successfully extract quality meteor echoes, *Yukimatu and Tsutsumi* [2002] developed a technique to reconstruct time series of quadrature outputs of the receiver (I (in phase) and Q (quadrature phase) signals) for each range gate by modifying the radar operating system (RADOPS) without affecting the existing SuperDARN ACF measurement technique. By using

---

[1]National Institute of Polar Research, Tokyo, Japan.
[2]Atmospheric Radar Systems, Thebarton, South Australia, Australia.
[3]Department of Physics and Astronomy, University of Leicester, Leicester, UK.

diffusion coefficients as a proxy of height information a semidiurnal tidal structure showing a downward phase propagation was obtained.

[5] In the present study we extend the work of *Yukimatu and Tsutsumi* [2002]. There are a few issues which were discussed but left unsolved by *Yukimatu and Tsutsumi* [2002]: (1) There is a possibility that meteor echoes received with the relatively strong backlobe and sidelobes contaminate the mainlobe echoes. Typical examples of the one way antenna pattern for SuperDARN radars when operated at 10 MHz are given by *Milan et al.* [1997], where the backlobe and the first sidelobe levels are around 10 dB and 14 dB down compared to the mainlobe, respectively. For both transmission and reception, they are 20 dB and 28 dB down, respectively. These values are not small enough when considering meteor echo intensity that can varies over 80 dB [*McKinley*, 1961]. An interferometer technique needs to be applied to eliminate these directional ambiguities. (2) The range resolution of normal SuperDARN operation is mostly 45 km, which is too coarse compared to a typical range resolution of $1-2$ km of a meteor radar measurement to resolve the fine height structures of atmospheric waves.

[6] The main arrays and subarrays of SuperDARN radars are used as a one dimensional interferometer to determine the elevation angles of echoes. SuperDARN interferometry has been used successfully, for example, to study the nature of backlobe echoes [*Milan et al.*, 1997], to separate meteor, E region and F region echoes [*André et al.*, 1998], and to investigate E region echoes in detail [*Milan et al.*, 2004]. Therefore, the aforementioned issue 1 can be dealt with using the existing interferometer technique. However, no technique to largely improve the range resolution of SuperDARN had been devised. To overcome this, we recently developed two ranging techniques, oversampling and frequency domain interferometry (FDI) [e.g., *Kudeki and Stitt*, 1987], and coded them in RADOPS. These new ranging techniques, especially the FDI, are thought to be useful not only for meteor observations but also for the study of fine spatial structures in E and F region echoes. In the following we first describe the experimental setup of the new observation technique in section 2. The obtained meteor distributions and preliminary results of wind measurements are shown in section 3. Finally concluding remarks are given in section 4.

2. Experimental Setup

[7] We have added an oversampling capability into the RADPOS, in which the signal is oversampled every 15 km even when the original sampling is every 30 or 45 km corresponding to a radar pulse width of 200 or 300 μs, respectively. Since the meteor trail is a discrete target, oversampling gives a better range estimate for such

targets. The range resolution is further improved using a moment method as described in section 3. In order to minimize the additional data size the new RADOPS is designed to oversample the radar signal only after the first transmitting pulse of each multipulse sequence.

[8] Further we employed another technique for accurate range determination: frequency domain interferometry (FDI). FDI is based on the use of slightly different multiple transmitting radio frequencies and can resolve fine structure in a range gate. The techniques have been applied to atmospheric radars such as MST radars to study layered structures and turbulence in the atmosphere [e.g., *Kudeki and Stitt*, 1987; *Luce et al.*, 2001]. FDI can be applied to SuperDARN observations if targets are discrete or there are highly inhomogeneous plasma structures in a range gate.

[9] Since we can assume that for most cases only one meteor appears in a certain range at the same time. the use of two frequencies is enough to resolve the position of the meteor trail in the range gate. It is possible that there exist more than one meteor trails at the same time in the same range gate although there is a small chance for that. In such a situation both oversampling and two-frequency FDI fail to estimate the real range.

[10] Here we describe the situation where we use two radio frequencies, f_1 and f_2 (corresponding wave lengths of λ_1 and λ_2). If the signal to noise ratio (SNR) is large enough and the difference in the wave numbers within one range gate is less than 0.5, the real range can be resolved without any ambiguities.

$$dR \mid \frac{1}{\lambda_1} - \frac{1}{\lambda_2} \mid < 0.5 \qquad (1)$$

or

$$|f_1 - f_2| = df < \frac{c}{2dR} \qquad (2)$$

where dR, c and df are the range resolution, the speed of the radio wave and the absolute difference between the two radio frequencies. Since we use the range resolution of 45 km in the present study, the maximum frequency difference is 3.3 kHz. We adopted 3 kHz for the difference in the experiment. This choice means that the FDI phase values change 360 degrees every 50 km (= $c/(2df)$).

[11] In order to conduct ACF operation the radio frequency should not be changed within one pulse sequence of 100 ms long. Thus our design of the FDI operation is to switch the radio frequency every pulse sequence. One thing to note is that the life time of the phenomenon of interest (here the duration of meteor echoes) should be longer than at least two pulse sequences, that is, 0.2 s, in order to apply the two frequency FDI. Also note that a phase shift caused by Doppler frequency shift should be corrected before estimating FDI phase values. Because of
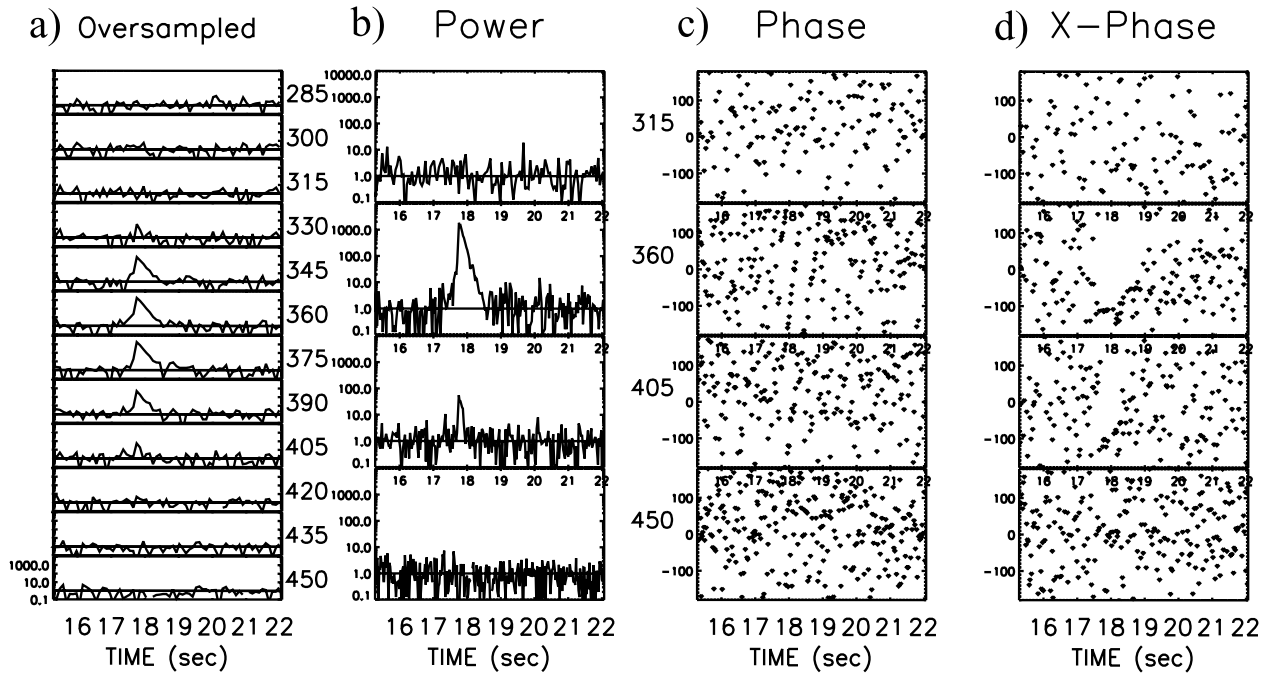
Figure 1. A typical example of time series of meteor echoes. (a) Echo power oversampled every 15 km at ranges of (top) 285 to (bottom) 450 km. (b) Echo power sampled every 45 km. (c) Phase corresponding to power series (Figure 1b). (d) Interferometer phase sampled every 45 km. The echo power (Figures 1a and 1b) is on a log scale.

the nature of meteor echoes their durations are often less than 0.2 s. This is an unavoidable limitation under the current SuperDARN operation. In this sense the over-sampling technique is thought to be superior to the FDI technique for meteor observations. In other words the FDI technique is more suitable for normal SuperDARN field aligned irregularity echoes in E and F regions, which usually have longer durations than two pulse sequences, but at the same time a careful approach would be necessary by checking each raw ACF or time series before the FDI is applied. In the upgraded RADOPS the interferometer data, which is the phase difference between the main arrays and subarrays, can also be stored in the time series data.

[12] The experiment was conducted using CUTLASS Iceland East (73.7°N, 20.5°W) and Finland (62.3°N, 26.6°E) radars of Leicester University between 22 UT of 6 February and 22 UT of 10 February 2004. Time series are not available over the period 12–18 UT, 8 February, when the radars were used for another experiment. Both radars were operated under the stereo mode [*Lester et al.*, 2004], in which the oversampling was conducted in the first channel (Channel A) and the FDI was carried out in the second (Channel B). The maximum sampling range was 540 km until 12 UT,

8 February, and then extended to 1440 km after 18 UT, 8 February. The center frequencies employed were within 11.075–11.275 MHz and 10.155–10.655 MHz for the Finland and Iceland radars, respectively. The interferometer spacings are 185 m and 100 m for the Finland and Iceland radars, respectively. All the raw time series during the experiment were stored for offline processing.

3. Results

3.1. Ranging of Meteor Echoes

[13] Figure 1 shows an example of the time series of a meteor echo. The echo is detected at the ranges of 360 km and also 405 km in the original 45 km resolution data (Figure 1b). In the oversampled series (Figure 1a), the meteor is seen at many more ranges between 330 and 405 km with the largest power around 360 km and the smallest at 330 and 405 km. We employed a moment method to further increase the accuracy of the range estimation [e.g., *Woodman*, 1985], in which 7 ranges around the range with the peak echo power were averaged after they were weighted with the corresponding echo power. The estimated range for the echo in Figure 1 is 366 km. In Figure 1c, the Doppler frequency shift is
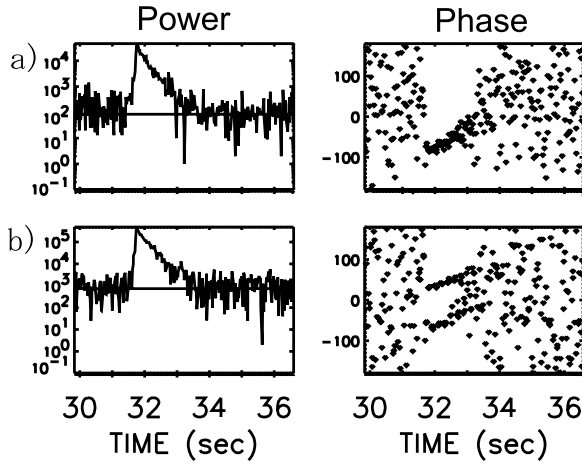
Figure 2. (a) Power and phase of a typical underdense meteor echo in the case of a single radio frequency measurement. (b) Same as Figure 2a in the case of a two-frequency measurement (FDI). The horizontal lines in the power series indicate the noise level.

clearly seen as a linear variation of phase with time. Figure 1d is the phase difference between the main and the subarray. In the second top plot the phase values during the meteor occurrence of around 18 s are almost constant around −100 degrees while they are quite random before and after the period.

[14] We now demonstrate the performance of the FDI technique. Figure 2 shows a meteor echo simultaneously observed by the stereo channels A and B, where the FDI was applied to channel B. The time evolution of the echo power looks almost identical. The somewhat different echo power between the two is thought to be due to the different gain setting of the two channels. The phase values show almost the same Doppler frequency shift around 32–33 s. It is noteworthy that the FDI phase values form two groups which correspond to the two radio frequencies separated by 3 kHz. The difference between the two phase groups gives the position of the meteor trail inside the 45 km range gate.

[15] Figure 3 compares the oversampling and FDI for the Finland radar observation of all meteors with a peak SNR more than 10 dB on 9 February 2004. Figure 3 (top) shows a scatterplot of the oversampled ranges and FDI phase values. It is clearly seen that the FDI phase values linearly change with the oversampled ranges. As described in section 2, 2π ambiguities appear in the FDI phase every 50 km corresponding to the frequency difference of 3 kHz, which is, however, longer than the range resolution of 45 km and can resolve the meteor position in the corresponding range gate without any ambiguities if the SNR is high enough. Note that the FDI phases are usually offset and need to be calibrated before

converted to range values [e.g., *Kudeki and Stitt*, 1987]. In the present study the oversampled ranges are actually used to obtain reasonable range values from the FDI information. The phase offset was estimated to be 150 degrees. The oversampled and FDI ranges are compared in Figure 3 (bottom). Ranges estimated by the two techniques agree very well. When the FDI phases are not calibrated, the values zigzag on the plot every 50 km and are not distributed along a straight line.

[16] We estimated the accuracy of our ranging techniques and the dependency on SNR through the comparison between the two techniques. Histograms of differences
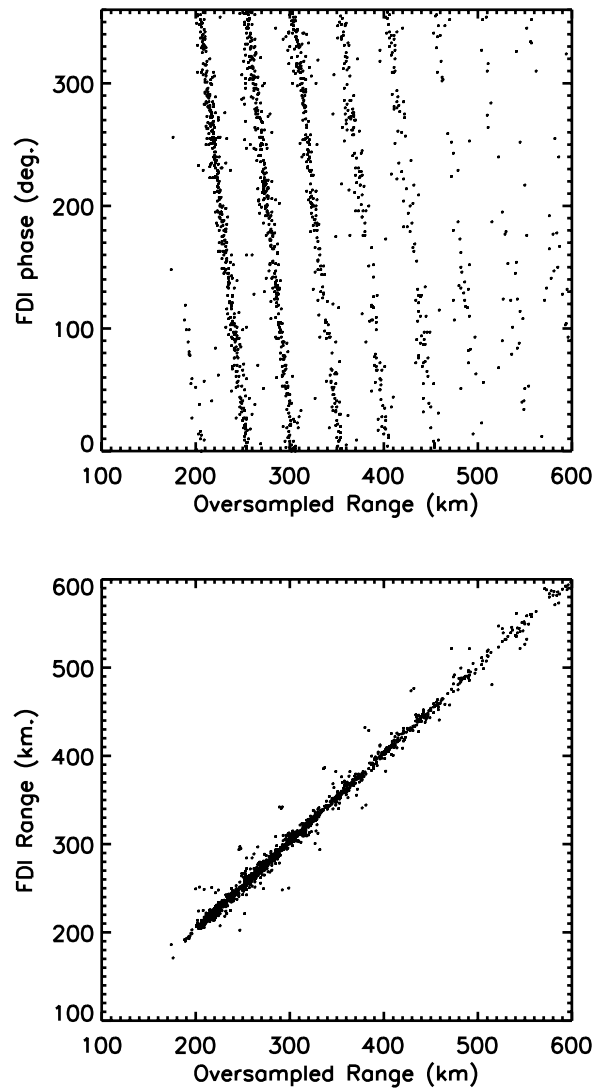

Figure 3. (top) Comparison between the oversampled ranges and FDI phase values based on the Finland radar observations made on 9 February 2004. (bottom) Comparison between the oversampled and FDI ranges.
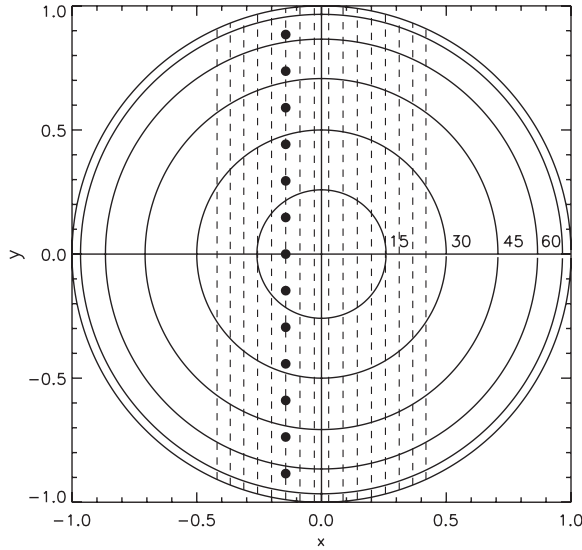
Figure 4. Schematic diagram showing the 16 fan beams of a typical SuperDARN radar. Horizontal two components of the directional vector of the beam patterns are plotted as dashed lines. Circles indicate zenith angles at every 15 degrees. Dots demonstrate how ambiguities of arrival angles of echoes appear in the case of an interferometer with a spacing 6.8 λ, which corresponds to the case in which the Finland radar is operated at a frequency of around 11 MHz.

between the two sets of range estimates were produced for Finland radar observations (not shown). They showed Gaussian distributions centered around 0 km with standard deviations of 12.3 km, 8.5 km and 6.3 km, for three SNR ranges of 5–10 dB, 10–15 dB and 15–20 dB, respectively. These standard deviations are thought to be the square root of the sum of the two independent range estimation errors. By assuming that the range estimation errors of the two techniques are the same, the errors are evaluated as 8.7 km, 6.0 km and 4.5 km for the three SNR groups, respectively. In the case of the SNR of 0–5 dB the difference histogram still shows a Gaussian shape and it seems that FDI ranges can be resolved without the 50 km ambiguities for many meteors, but the agreement between the two techniques becomes increasingly worse. For meteors with SNR greater than 10 dB, which are used for wind analyses, the average range error is 5.3 km.

[17] One can notice that although almost all the points are aligned on the line in Figure 3, there are some outlying points which are not. These erroneous estimations seem to be caused by our preliminary FDI ranging algorithm. When the range of a meteor trail falls around the border of two 45-km-wide-range gates, the meteor echo power of the two range gates is almost the same.

Thus, if the initial selection of the range gate in which the real range lies is wrong, it leads to a large estimation error. However, these errors can be avoided by comparing the echo power of the adjacent range gates. The FDI algorithm will be revised in future studies.

3.2. Angles of Arrival Estimation

[18] Since the shape of the SuperDARN antenna beam, so-called 'fan beam,' is corn-shaped in real space [*André et al.*, 1998] and is not easily drawn on the two-dimensional surface, we introduce the directional vector of the antenna beam to simplify the discussion. When thinking of a sharp pencil beam pointing at the azimuth and zenith angles of (ϕ, θ), the two horizontal components (x, y) of the directional vector are $\sin(\phi)\sin(\theta)$ and $\cos(\phi)\sin(\theta)$, and can be plotted as a dot in a polar diagram such as Figure 4. In the case of a fan beam the pattern is simply expressed as a straight line as also shown in Figure 4, in which the fan beam number i (0–15) of SuperDARN radars is expressed as

$$x = \sin\{bmsep \cdot (i - 7.5)\} \qquad (3)$$

[19] The term inside the brackets is in degrees. The value, 'bmsep,' is the beam separation and is 3.24 degrees for CUTLASS radars.

[20] By assuming that echoes are observed by the fan beam, the angle of arrival (AOA) of each echo can be determined by using the interferometer phase. Because the spacings of the interferometer of the SuperDARN radars are much larger than a half wave length, multiple directional ambiguities exist for most of the cases. An example is demonstrated in Figure 4 as solid circles, in which a meteor echo is assumed to be observed with the beam 5 of the Finland radar operated at a radar frequency of 11 MHz. More than ten AOA candidates exist in this case. However, since almost all the meteor echoes in HF bands are detected at a height between 70 and 120 km, the real AOA can be determined when only one candidate exists in this height range although this is not always the case.

[21] Before showing the spatial distribution of observed meteor echoes we describe range and interferometer phase calibrations, which were necessary to obtain a realistic spatial distribution of meteor echoes. The range offset of −50 km was employed for both the radars. This is a reasonable value assuming the delay caused by the matched filter designed for the 300 μs wide transmitting pulse. This range correction is important especially for short range echoes, for which the estimated height become unrealistically high without the range correction. The interferometer phases were carefully calibrated in such a way that the estimated meteor heights became distributed horizontally. The estimated phase offsets for the first
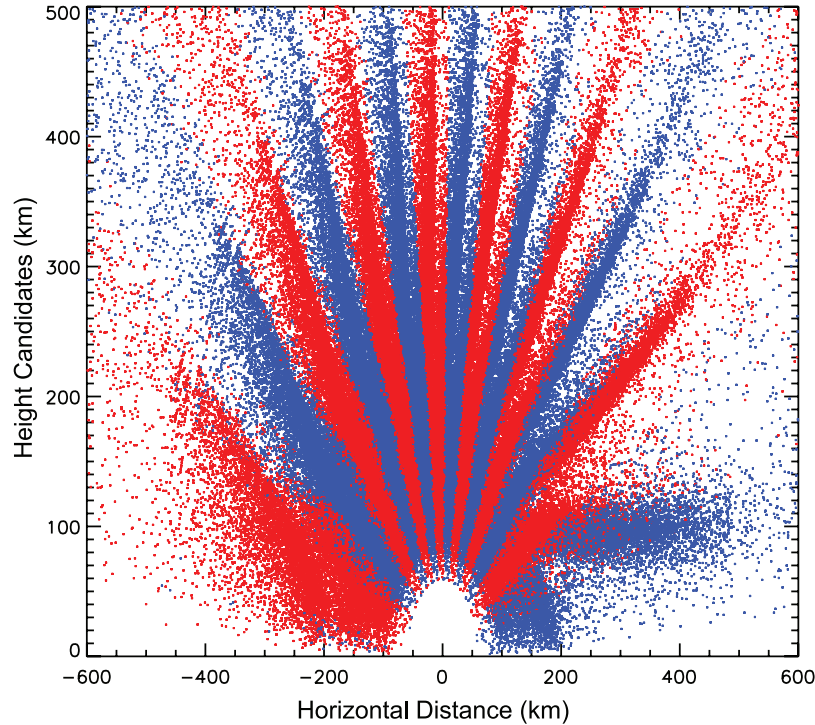
Figure 5. Height candidates versus horizontal distance distribution of meteor echoes observed by the Finland radar on 6−10 February 2004. The positive horizontal distance is the bore site direction.

channel of Finland and Iceland radars are 230 and 220 degrees, respectively. These values can depend on the operating frequency, and it will be necessary to estimate appropriate values for other operation frequencies. Although it is not very easy to evaluate how accurately these offsets can be corrected, the spatial distribution of meteor echoes can look distorted when the range and phase offset values are changed by more than about 5 km and 5 degrees.

[22] Figures 5 and 6 show the cross sections of height candidates and horizontal distance for the Finland and Iceland radar observations, respectively. Horizontal distance along each beam direction is chosen for the abscissa so that echoes for all the 16 beams can be plotted in one plot. Note that all the echoes are assumed to be detected through the radar antenna main beam expressed in equation (3). In order to demonstrate how AOA ambiguities appear all the possible AOAs are plotted although the distributions well above 100 km cannot be real AOAs. The color is changed every time the interferometer phase is incremented by 2π (rad.). The number of ambiguities for each echo depends on the spacing of the interferometer and operating frequency. In this experiment it is about 14−15 and 7 for the Finland and Iceland radars, respectively. Because of these ambiguities, only 30% and 40% of the total echoes for

Finland and Iceland radars, respectively, have a unique AOA solution even under the assumption that meteor echoes distribute between 70 and 120 km altitudes. However, the echoes which align horizontally around 70−120 km with a positive horizontal distance correspond to the real distribution. Almost all the others are AOA ambiguities. The corresponding area in the case of the Iceland radar is marked as the area A in Figure 6. The number of underdense type meteor echoes in the regime is about 3000 a day, which is about 70% of the total meteor echoes.

[23] It is noteworthy that in the case of the Iceland radar there is small population of echoes which distribute around 100 km altitude in the negative horizontal distance regime denoted as the area B in Figure 6. These echoes correspond to those in the area C in Figure 6 and are obviously not the AOA ambiguities of the area A echoes. To better understand the nature of the echoes in the area B (or C), the radial wind velocities of the echoes in the areas A and B are plotted together in Figure 7. The echoes in area A (red dots) show a sinusoidal variation with time, probably exhibiting a semidiurnal tidal activity while the echoes in area B mostly indicate an opposite sense to those in area A with some echoes distributing randomly. These features indicate that the echoes in areas A and B are mostly detected by the main beam and the
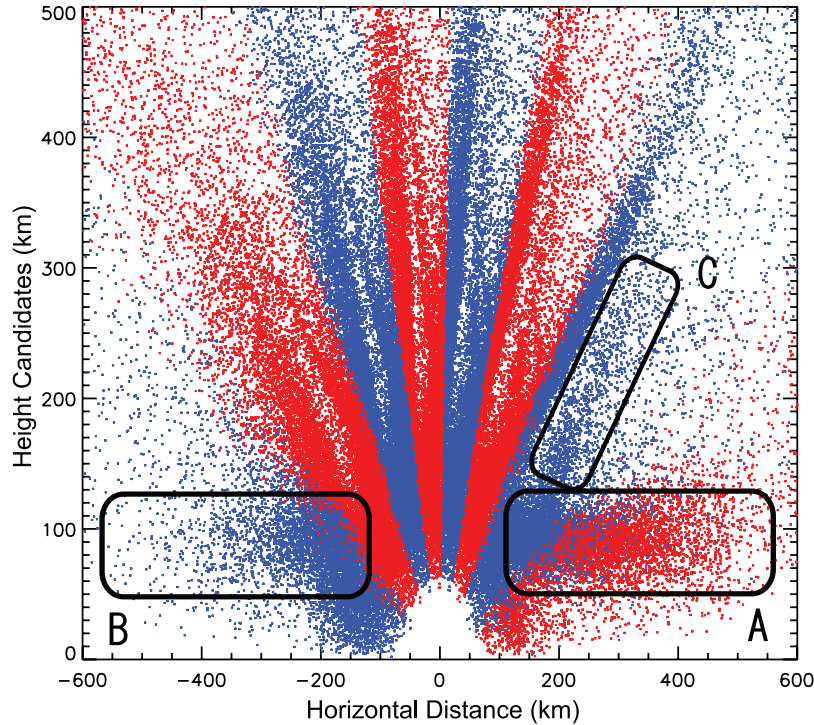
Figure 6. Same as Figure 5 except for the Iceland radar observations. See text for the explanation of areas A, B, and C.

backlobe, respectively. Note that some strong echoes may be detected by sidelobes although we cannot determine their real AOAs because the SuperDARN interferometer is only one-dimensional at the moment. The randomness seen in area B echoes in Figure 7 is thought to be caused by those sidelobe echoes. Since the difference in gain between the backlobe and sidelobes is much smaller than that between the mainlobe and nonmainlobes, the effect of sidelobe echoes is reasonably considered to be more enhanced in area B than area A. In the case of the Finland radar (Figure 5) there is no

such population as area C of Figure 6. The radial wind velocity plot for the Finland radar (not shown) does not show features seen in Figure 7 either. Therefore, the effect of nonmainlobe echoes for the Finland radar seems minor compared to the Iceland radar. This difference between the two radars is seemingly caused, at least partly, by differences in the bore site direction, radar frequency, antenna pattern and also surrounding ground condition.

[24] Before leaving this section, elevation angle estimation errors are discussed. First, interferometer phase
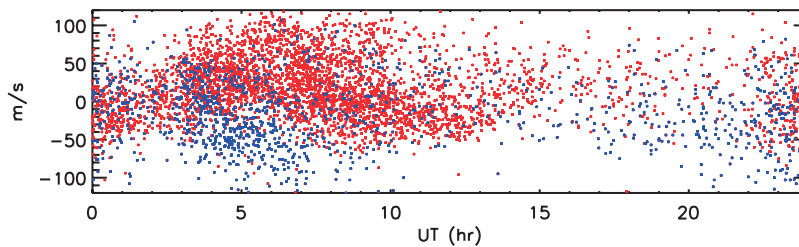

Figure 7. Radial wind velocities of the Iceland radar observed on 6–10 February 2004. The red and blue dots correspond to echoes in the areas A and B of Figure 6, respectively.
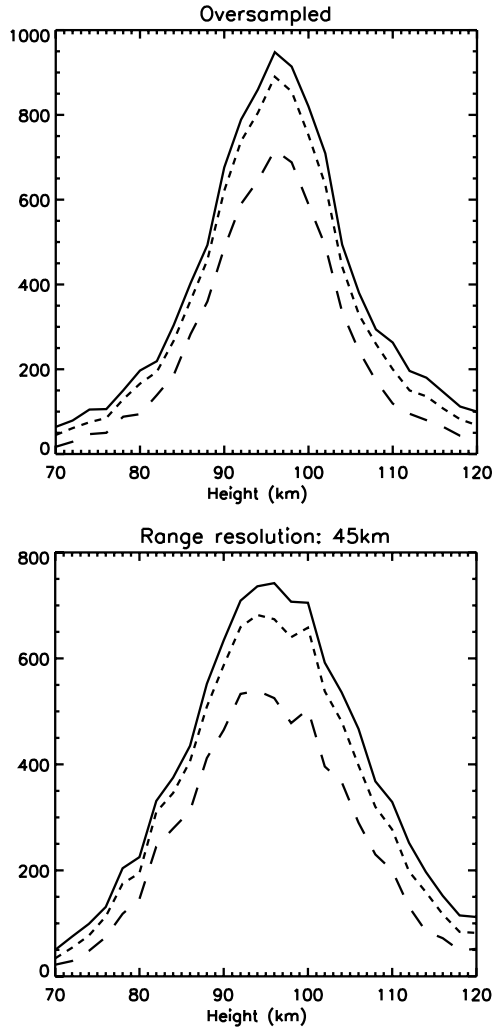
Figure 8. Height distributions of meteor echoes observed by the Finland radar on 6–10 February 2004. Three lines correspond to meteors which were detected at the ranges equal to or less than 535 km (solid), 355 km (dotted), and 265 km (dashed). These ranges are corrected by −50 km as described in section 3.1. (top) Estimated using oversampled ranges. (bottom) Estimated using the original range resolution of 45 km.

errors were estimated for echoes with SNR greater than 10 dB using the Finland radar data. Then an average was found to be 16 degrees. Since the majority of echoes are distributed at elevation angles of around 20–30 degrees, the corresponding error for elevation angles is about 0.8 degrees for the Finland radar. Assuming the same phase error for the Iceland radar, the corresponding elevation angle error is 1.7 degrees. The difference between the two radars is due to the difference in the interferometer spacing and radar frequency.

3.3. Height Distribution

[25] The height distribution of the Finland radar echoes is shown in Figure 8, where all the echoes which appeared in the main beam regime are used. Three lines correspond to three distributions with maximum sampling ranges of 535 km (solid), 355 km (dotted) and 265 km (dashed), respectively. The correction of −50 km described in section 3.2 is made for these three ranges. As indicated in Figure 3 only a small number of echoes are observed at ranges greater than 500 km. Nearly 70% of echoes are observed within 265 km. This range distribution seems to be mostly due to the fact that the echo power is inversely proportional to the cube of the range [e.g., *McKinley*, 1961] and also due to the fact that far range meteor echoes arrive from a very low elevation angle, at which the antenna gain becomes increasingly low. The range distribution observed here is very similar to that obtained by *André et al.* [1998], in which they successfully separate meteor echoes from E and F region echoes using SuperDARN interferometry.

[26] Note here that although the height distribution with the maximum sampling range of 535 km indicates some meteor population below 70 km and above 120 km, it is probably caused by somewhat poorer AOA estimation for far range echoes. Therefore caution should be made when using far range meteor echoes for wind analysis. Height errors can be calculated using the range and elevation angle errors estimated in sections 3.1 and 3.2. At the elevation angle of 20–30 degrees, in which most echoes distribute, the height error for echoes with SNR of greater than 10 dB is around 4 km. At the elevation angle of 15 degrees the value gets increasingly large and is nearly 9 km.

[27] The mean height and standard deviation for the height distribution with the maximum sampling range of 265 km (dashed line in Figure 8) are 96 km and 8.6 km, respectively. This mean value shows good agreement with those of previous SuperDARN meteor studies, 94 ± 3 km [*Hall et al.*, 1997], where ±3 km is not a standard deviation of height distribution but an estimation error of the mean height, and 97 km [*Yukimatu and Tsutsumi*, 2002]. A mean height around these values is an expected value for HF operation being between typical VHF and MF meteor observations of around 90 km and 100 km, respectively [*Nakamura et al.*, 1991; *Holdsworth et al.*, 2004; *Tsutsumi and Aso*, 2005].

[28] For comparison the height distribution using the original 45 km range resolution is shown in Figure 8 (bottom). Although the mean height is the same value of 96 km with the oversampled result, the distribution is obviously wider with the standard deviation of 10.2 km.
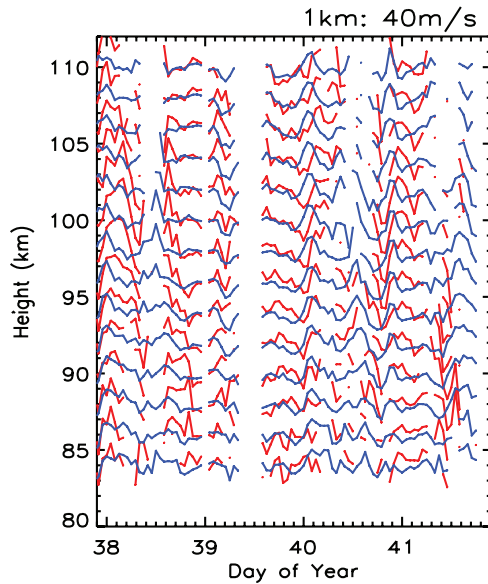
Figure 9. Eastward (red) and northward (blue) wind components observed with the Finland radar on 6–10 February 2004; 1 km corresponds to 40 m/s. No time series data are available during 12–18 UT, 8 February, because the radar was operated in another observation mode during the period.

3.4. Wind Velocity Estimation

[29] Horizontal wind velocities were estimated using the same technique employed for conventional meteor radars. As the vertical wind velocity is generally much smaller than the horizontal components for atmospheric phenomena considered here, it was reasonably neglected in the wind estimation. Winds are estimated for time height bins with dimension of 2 hours and 4 km. A horizontal wind vector was fitted by employing a least squares method only when the number of underdense meteor echoes in each bin was equal to or more than five. The bin was shifted by 1 hour and/or 2 km (i.e. half the bin size), and the calculation was repeated. The estimated eastward and northward components for the Finland radar observation are shown in Figure 9. When the confidence interval of each wind estimate is more than 20 m/s, the wind value is not plotted in Figure 9. Velocities are estimated at the height range of 84–110 km. Clear and complicated wave structures are seen in both components with a semidiurnal variation seemingly dominant. It is noteworthy that the northward component generally leads the eastward component, for example around 0 UT on day 40 (9 February), exhibiting the commonly observed nature of atmospheric waves in the northern hemisphere.

[30] The eastward winds are obviously noisier than the northward winds because the bore sites of the SuperDARN radars are mostly poleward and the projection of east westward flow to the radial wind velocity is relatively small. Further, wind velocities in the evening were not very easy to estimate because the echo rates were much less than those in morning hours. Typical values of the confidence intervals for the estimated wind velocities are less than 5 m/s and 10 m/s in morning hours for the northward and eastward wind velocities at around 96 km altitude, respectively. Those of evening hours become worse and often excess 20 m/s for the eastward component. Readers should note that meteor echo rates show large seasonal and diurnal variations. *Singer et al.* [2004] studied diurnal and annual meteor echo rates in the Arctic using meteor radars. In the northern high latitudes the seasonal variation shows a peak occurrence around summer months and a sharp minimum rate in February to March. The maximum to minimum ratio is nearly 3. The diurnal variation with a morning maximum and evening minimum is mostly enhanced in January and February. Therefore, the early February observation period of the present study is expected to be the worst to demonstrate the performance of the SuperDARN meteor wind observation technique. Nevertheless, clear wave structures are depicted as seen in Figure 9 even under such conditions.

4. Conclusions

[31] In the present study we have upgraded the SuperDARN raw time series analysis technique originally developed by *Yukimatu and Tsutsumi* [2002]. *Yukimatu and Tsutsumi* [2002] modified the radar operating system (RADOPS) of SuperDARN to store raw time series of I/Q samples without affecting the existing autocorrelation function analysis (ACF). We further modified the RADOPS and added the following capabilities: (1) Interferometer phase values can be stored in the raw time series data. (2) Even when the range resolution of the existing ACF operation is 30 or 45 km, the receiver output can be oversampled every 15 km (100 μs) after the first transmitting pulse of the multipulse sequence. (3) The radar operating frequency can be specified every pulse sequence so that frequency domain interferometer (FDI) techniques, which had never been tried using SuperDARN radars, can be applied.

[32] After these modifications we conducted test experiments using the CUTLASS Iceland East and Finland radars in February 2004 and extracted meteor echoes from the stored raw time series. The oversampled and FDI ranges agreed very well. The ambiguities of angle of arrival of echoes were mostly removed using the interferometer data. Reflection heights of underdense

meteor echoes show a reasonable distribution with a peak value around 96 km, which is between those of typical VHF and MF radar meteor measurements. Horizontal two dimensional wind velocities were estimated. Clear atmospheric wave structures were observed showing a typical phase relation in the northern hemisphere that the northward component lead the eastward one.

[33] In deducing realistic ranges and angles of arrival of meteor echoes, observed range and interferometer phase values needed to be calibrated based on the well known fact that meteor echoes are distributed horizontally around 70–120 km altitude. In other words this indicates that meteor echoes are useful to calibrate SuperDARN radars [*Milan et al.*, 2004].

[34] We successfully distinguished mainlobe and backlobe meteor echoes using the SuperDARN interferometer data. However, we still cannot discard the possibility of the existence of sidelobe echoes and do not know their possible effects on estimated wind information although the proportion of those echoes is thought to be small. In order to investigate their effects we are planning to detect simultaneous meteor echoes using collocated Syowa SENSU SuperDARN radars and MF radar at Syowa (69°S, 39°E) and compare results between the two radar systems. The MF radar is equipped with 4 receiving antennas and receivers with full interferometry capability and can determine AOA of meteor echoes with much fewer ambiguities [*Tsutsumi and Aso*, 2005]. As the comparison is beyond the scope of this paper, we leave it as a future study.

[35] The frequency domain interferometer capability coded in RADOPS was tested successfully for meteor observations. However, this technique is thought to be more useful for E and F region study to detect discrete targets or inhomogeneous structures within each range gate. We used only two frequencies in the present study because we assumed that the number of targets (meteor trails) in a range gate was one. However, when the number of radio frequencies used is n and the correlation time of the target is long enough, n-1 targets in a bin can be resolved in theory [e.g., *Luce et al.*, 2001]. Because the frequency offset for SuperDARN FDI of only 3 kHz or so is negligible compared with the operation frequency between 8 and 20 MHz, the Doppler parameters estimated from ACFs of the different FDI frequencies are virtually the same and can be incoherently integrated in the same manner with the current one frequency operation without causing any problems. Thus, we suggest that the FDI technique be adopted as a standard technique of the SuperDARN observation. Recently we started a coordinated experiment with the EISCAT heater facility to study the nature of the heater echoes with high time and spatial resolutions. Those results will be presented elsewhere.

[36] The techniques developed by *Yukimatu and Tsutsumi* [2002] and the present study are believed to further expand the capability of SuperDARN radars. A network observation of mesopause region and E and F regions using these techniques will greatly benefit the study of these regions.

References

André, D., G. J. Sofko, K. B. Baker, and J. MacDougall (1998), SuperDARN interferometry: Meteor echoes and electron densities from ground scatter, *J. Geophys. Res.*, *103*, 7003–7015.

Chisham, G., et al. (2007), A decade of the Super Dual Auroral Radar Network (SuperDARN): Scientific achievements, new techniques and future directions, *Surv. Geophys.*, *28*, 33–109, doi:10.1007/s10712-007-9017-8.

Greenwald, R. A., K. B. Baker, R. A. Hutchines, and C. Hanuise (1985), An HF phased-array radar for studying small-scale structure in the high latitude ionosphere, *Radio Sci.*, *20*, 63–79.

Greenwald, R. A., et al. (1995), DARN/SuperDARN: A global view of the dynamics of high-latitude convection, *Space Sci. Rev.*, *71*, 761–796.

Hall, G. E., J. W. MacDougall, D. R. Moorcroft, J. P. St.-Maurice, A. H. Manson, and C. E. Meek (1997), SuperDARN radar observations of meteor echoes, *J. Geophys. Res.*, *102*, 14,603–14,614.

Holdsworth, D. A., I. M. Reid, and M. A. Cervera (2004), Buckland Park all-sky interferometric meteor radar, *Radio Sci.*, *39*, RS5009, doi:10.1029/2003RS003014.

Kudeki, E., and G. R. Stitt (1987), Frequency domain interferometry: A high resolution radar technique for studies of atmospheric turbulence, *Geophys. Res. Lett.*, *14*, 198–201.

Lester, M., et al. (2004), Stereo CUTLASS—A new capability for the SuperDARN radars, *Ann. Geophys.*, *22*, 459–473.

Luce, H., M. Yamamoto, S. Fukao, D. Helal, and M. Crochet (2001), A frequency domain radar interferometric imaging (FII) technique based on high-resolution methods, *J. Atmos. Sol. Terr. Phys.*, *63*, 221–234.

McKinley, D. W. R. (1961), *Meteor Science and Engineering*, McGraw-Hill, New York.

Milan, S. E., T. B. Jones, T. R. Robinson, E. C. Thomas, and T. K. Yeoman (1997), Interferometric evidence for the observation of ground backscatter originating behind the CUTLASS coherent HF radars, *Ann. Geophys.*, *15*, 29–39.

Milan, S. E., M. Lester, T. K. Yeoman, T. R. Robinson, M. V. Uspensky, and J.-P. Villain (2004), HF radar observations of high-aspect angle backscatter from the E-region, *Ann. Geophys.*, *22*, 829–847.

Nakamura, T., T. Tsuda, M. Tsutsumi, K. Kita, T. Uehara, S. Kato, and S. Fukao (1991), Meteor wind observations with the MU radar, *Radio Sci.*, *26*, 857–869.

Singer, W., U. von Zhan, and J. Weiß (2004), Diurnal and annual variations of meteor rates at the arctic circle, *Atmos. Chem. Phys.*, *4*, 1355–1363.

Tsutsumi, M., and T. Aso (2005), MF radar observations of meteors and meteor-derived winds at Syowa (69°S, 39°E), Antarctica: A comparison with simultaneous spaced antenna winds, *J. Geophys. Res.*, *110*, D24111, doi:10.1029/2005JD005849.

Woodman, R. F. (1985), Spectral moment estimation in MST radars, *Radio Sci.*, *20*, 1185–1195.

Yukimatu, S. A., and M. Tsutsumi (2002), A new SuperDARN meteor wind measurement: Raw time series analysis method and its application to mesopause region dynamics, *Geophys. Res. Lett.*, *29*(20), 1981, doi:10.1029/2002GL015210.

————————

D. A. Holdsworth, Atmospheric Radar Systems, 1/26 Stirling Street, Thebarton, SA 5013, Australia.

M. Lester, Department of Physics and Astronomy, University of Leicester, Leicester LE1 7RH, UK.

M. Tsutsumi and A. S. Yukimatu, National Institute of Polar Research, 1-9-10 Kaga, Itabashi, Tokyo 173-8515, Japan. (tutumi@nipr.ac.jp)